https://doi.org/10.2352/ISSN.2470-1173.2020.14.COIMG-263

Comparing Classification Performance of Mueller Matrix Parameters for Diffuse Materials

Lisa W Li, Meredith Kupinski, Madellyn Brown, Russell Chipman

Abstract

This work compares the material classification performance of Mueller matrix polarization imaging to RGB imaging. White painted wood and white fabric samples are selected to create a classification task that is challenging for RGB imaging. A Mueller Matrix Imaging Polarimeter with a 30° full field of view is used to capture the Mueller Matrix images at nominal red, green, and blue wavelengths across multiple specular scatter angles. A Bayesian ideal observer model is used to evaluate classification performance. Performance is quantified by the Area under (AUC) the Receiver Operating Characteristic (ROC) curve. An AUC = 1 is perfect detection and AUC = 0.5 is the performance of guessing. The ensemble average AUC does not exceed 0.70 for RGB irradiance data. The ensemble average AUC for all 16 individual Mueller elements is greater than 0.95. Various combinations of Mueller matrix elements are also tested. Elements related to diattenuation and polarizance are nearly perfect classifiers for large scatter angles but the AUC minimum is 0.60 at 20°*. Depolarization index is the highest performing parameter out of all tested polarization parameters for scatter angles* $\geq 70^\circ$ *where AUC* $\geq$*0.98.*

Introduction

State of the art RGB image classification algorithms rely on neural networks analyzing materials within the context of object shapes and full scenes to determine material labels [9, 10]. This work demonstrates an advantage to using polarization measurements to distinguish diffuse materials which appear similar in traditional color images.

Previous work in polarization imaging focuses on differentiating metallic and dielectric materials in controlled manufacturing settings and outdoor scenes. Distinguishing dielectric from metallic materials can be accomplished using the degree of linear polarization (DoLP) in a specularly reflected beam [1, 2, 3, 4]. Differences in non-metallic materials has been demonstrated using only the irradiance parameter and two linear Stokes parameters [5, 6, 7, 8]. The four Stokes parameters describe all possible polarization states of light. A linear polarizer in front of a camera or a commercially available linear Stokes camera does not measure all of the Stokes parameters. The four Stokes parameters are defined as

$$\mathbf{S} = \begin{bmatrix} S_0 \\ S_1 \\ S_2 \\ S_3 \end{bmatrix} = \begin{bmatrix} P_H + P_V \\ P_H - P_V \\ P_{45^\circ} - P_{135^\circ} \\ P_R - P_L \end{bmatrix} \tag{1}$$

where $\mathbf{S}$ is called a Stokes vector and P is an irradiance measurement in units of W/m^2. The subscript on P denotes transmission through a polarization analyzer (*e.g.* filter): horizontal (H), vertical (V), 45°, 135°, right-circular (R), and left-circular (L). Linear light-matter interactions transform an incident polarization state to an exiting polarization state (*e.g.* reflected or transmitted). This linear transformation is calculated through matrix multiplication with the Stokes vector

$$\tilde{\mathbf{S}} = \begin{bmatrix} m_{00} & m_{01} & m_{02} & m_{03} \\ m_{10} & m_{11} & m_{12} & m_{13} \\ m_{20} & m_{21} & m_{22} & m_{23} \\ m_{30} & m_{31} & m_{32} & m_{33} \end{bmatrix} \mathbf{S} = \mathbf{M}(\theta, \gamma, \lambda)\mathbf{S}. \tag{2}$$

Here the 4×4 Mueller matrix (MM) $\mathbf{M}$ in general depends upon the angle of incidence θ, the scatter angle γ, and the wavelength of light λ. The MM of air is invariant to these parameters and is equal to the identity matrix, which arises naturally since propagation through free space should not affect the polarization state of light. The 16 individual elements m_{ij} are unitless. In this work the classification performance of certain MM elements and four polarization parameters (*i.e* combinations of MM elements) are reported: diattenuation, polarizance, a 3×3 sub-matrix of MM, and the depolarization index.

Diattenuation describes how much light is reflected or transmitted when specific polarization states are incident upon a material. Elements from the top row of the MM are are used to compute this parameter by

$$\begin{bmatrix} 1 \\ \mathbf{d} \end{bmatrix} = \begin{bmatrix} 1 \\ d_H \\ d_{45^\circ} \\ d_R \end{bmatrix} = \frac{1}{m_{00}} \begin{bmatrix} m_{00} \\ m_{01} \\ m_{02} \\ m_{03} \end{bmatrix}. \tag{3}$$

Here $\mathbf{d}$ is the diattenuation vector and d_H, d_{45}, and d_R are the scalar-valued horizontal, 45°, and circular components; respectively.

Polarizance is the fraction of radiant energy that becomes polarized from unpolarized incidence. The leftmost column of the MM is used to calculate this parameter

$$\begin{bmatrix} 1 \\ \mathbf{p} \end{bmatrix} = \begin{bmatrix} 1 \\ p_H \\ p_{45^\circ} \\ p_R \end{bmatrix} = \frac{1}{m_{00}} \begin{bmatrix} m_{00} \\ m_{10} \\ m_{20} \\ m_{30} \end{bmatrix}. \tag{4}$$

Here $\mathbf{p}$ is the polarizance vector and p_H, p_{45}, and p_R are the scalar-valued horizontal, 45°, and circular components; respectively.

The 3×3 sub-matrix of elements in the bottom-right corner of a MM is

$$\mathbf{M} = \begin{bmatrix} m_{00} & m_{01} & m_{02} & m_{03} \\ m_{10} & & & \\ m_{20} & & \tilde{\mathbf{M}} & \\ m_{30} & & & \end{bmatrix} = m_{00} \begin{bmatrix} 1 & \mathbf{d} \\ \mathbf{p} & \frac{1}{m_{00}}\tilde{\mathbf{M}} \end{bmatrix}. \tag{5}$$

Here $\tilde{\mathbf{M}}$ are nine MM elements from the bottom-right corner of a MM. Pure retarders have no diattenuation, polarizance, or depolarization; these materials are defined by a MM with a zero-valued $\mathbf{d}$, zero-valued $\mathbf{p}$, and a unitary $\tilde{\mathbf{M}}$. For more complicated materials, such as the wood and fabric used in this work, $\tilde{\mathbf{M}}$ is a confluence of polarization parameters, including retardance.

Depolarization index is a single summary value of MM depolarization. A depolarization index of 0 indicates a completely depolarizing MM; a value of 1 indicates a non-depolarizing MM [17, 19]. Depolarization index is defined as

$$\Delta = \sqrt{1 - \frac{F_D}{m_{00}^2}} \tag{6}$$

where

$$F_D = \frac{1}{3}\left(4m_{00}^2 - \sum_{i,j=0}^{3} m_{ij}^2\right). \tag{7}$$

The MM of any subject can be calculated from multiple images with known illumination and analyzed polarization states; recovering a MM requires a minimum of 16 measurements, but taking more measurements recovers a more robust MM [16]. Optimization of the illumination and measurement polarization states for specific classification tasks has been covered in previous work [15].

In this work the context of the materials within an image does not inform the classifier since performance is computed per pixel. To demonstrate the efficacy of MM imaging for classification tasks, this method is tested on an adversarial dataset of diffuse white materials which are similar in appearance. This dataset contains 7 wood and 7 fabric samples which is too small to train a deep convolutional neural network or other machine learning technique [11, 12]. The Bayesian observer is used to evaluate classification performance from an independent testing and training set.

Methods

This study focuses on an adversarial two-class data set consisting of painted wood planks and fabric samples selected to be similar in color and tone. The wooden planks are sanded and thinly coated twice with non-glossy white spray paint. The fabric samples are bleached and ironed. Pairs of white fabrics samples and white painted planks are imaged together in a custom bench top multi-spectral rotating retarder Mueller Matrix Imaging Polarimeter called the RGB950 [13] (Figure 1).

This polarimeter operates at 451nm, 524nm, and 662nm for the blue, green, and red wavelengths respectively. The samples are illuminated at varying angles of incidence from 10° to 65° in 5° steps, and a MM image is captured at the corresponding specular angle. Results are reported with respect to scatter angle γ between the source axis and the camera axis, which ranges from 20° to 130° in 10° steps. Polarization parameters are calculated for each image, and the same region of interest on the camera detector is selected for sampling each material at each scatter angle.

Each pixel on the MM image region of interest is treated as an individual sample and classified in a 2 alternative forced choice (2AFC) task. For a 2AFC task, the Bayesian ideal observer uses the probability distribution functions (PDFs) of the two classes to compute the highest possible classification performance for those distribution. Data from four paints and four fabrics are randomly selected to be used as training data to estimate the PDFs for the two classes. The remaining fabric and paint data are used for testing how generalizable those PDFs are for novel cases.

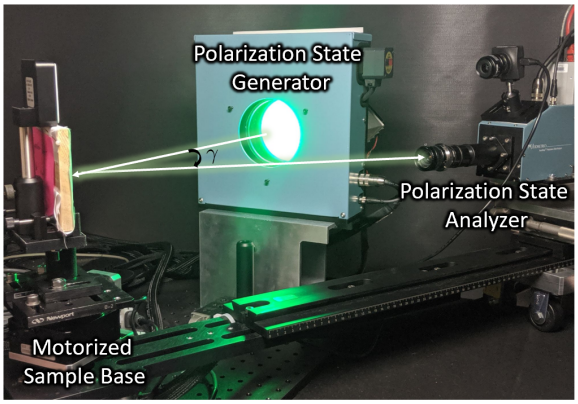

Figure 1. *RGB950: a Multi-spectral Rotating Retarder Imaging Mueller Matrix Polarimeter which operates at 451nm, 524nm, 662nm, and 947nm. The angle between the polarization state generator and polarization state analyzer is the scatter angle γ.*

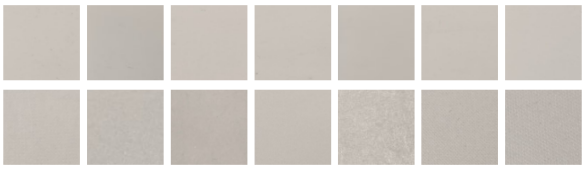

Figure 2. *Images of paint and fabric samples removed from their scene context. The top row is matte white paints: Ace Premium, Ace Rust-Oleum, Krylon ColorMax, Liquitex, Rust-Oleum, Rust-Oleum 2X, and Colorshot. The bottom row is fabrics: Wool, Felt, Cotton, 97% Cotton 3% Spandex, Silk, 60%Cotton 40% Polyester, and Polyester.*

The true positive fraction (TPF) is the proportion of fabric test data which has been correctly classified as fabric, and false positive fraction (FPF) is the proportion of paint test data which has been classified incorrectly as fabric. The TPF and FPF plotted together as the classification threshold is varied form a receiver operating characteristic (ROC) curve. The area under this curve (AUC) is the single value metric used to report performance. Two identical, indistinguishable distributions results in an AUC of 0.5, which indicates guessing performance. Two completely distinct distributions without crossover result in an AUC of 1, indicating perfect performance.

The Bayesian ideal observer maximizes the AUC, as well as other task-based figures of merit using the log of the ratio of the likelihoods as a test statistic [18]. This log likelihood ratio is defined as

$$\Lambda(\mathbf{g}) = \ln[pr(\mathbf{g}|1)] - \ln[pr(\mathbf{g}|2)] \tag{8}$$

where $\mathbf{g}$ is the vector of classification parameters for a single pixel. This equation simplifies for normal likelihoods to

$$\Lambda(\mathbf{g}) = (\mathbf{g}-\bar{\mathbf{g}}_2)^t \mathbf{K}_2^{-1}(\mathbf{g}-\bar{\mathbf{g}}_2) - (\mathbf{g}-\bar{\mathbf{g}}_1)^t \mathbf{K}_1^{-1}(\mathbf{g}-\bar{\mathbf{g}}_1) \tag{9}$$

where terms that do not depend on $\mathbf{g}$ have been dropped and the covariance matrix of the c^{th} class simplifies to $\mathbf{K}_c = \sigma_c^2\mathbf{I}$. The mean $\overline{\mathbf{g}_c}$ and variance σ_c^2 are calculated using training data. The likelihood model is further simplified by assuming each parameter is independent and identical distributed (i.i.d). The simplified expression for log-likelihood ratio is

$$\Lambda(\mathbf{g}) = \frac{||\mathbf{g}-\overline{\mathbf{g}}_2||^2}{\sigma_2^2} - \frac{||\mathbf{g}-\overline{\mathbf{g}}_1||^2}{\sigma_1^2} \tag{10}$$

where $||.||^2$ denotes the length-squared of the vector.

Results

The irradiance for the individual color channels and the combined RGB image is used to set a performance benchmark; see Figure 3. The average AUCs over all incident angles is 0.69 for red, 0.65 for green, 0.69 for blue, and 0.67 for all RGB color channels combined. The AUC dependence on scatter angle is not statistically significant which can be seen by the large error bars in Figure 3. The average AUC from $20^\circ - 130^\circ$ scatter angle is within one standard deviation from a given scatter angle compared to the others.

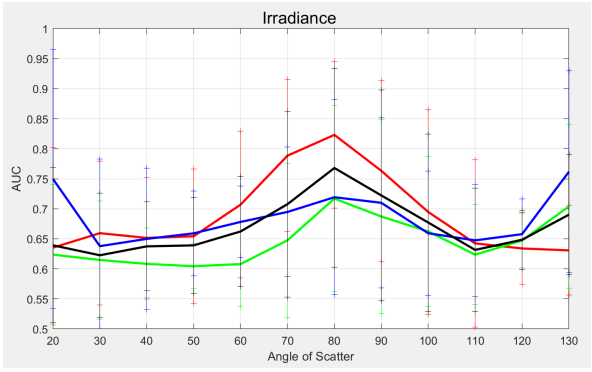

Figure 3. *Area under the curve (AUC) for traditional irradiance images. Error bars indicate first standard deviation calculated from a 5-fold cross validation. Red: 662nm, Green: 524nm, Blue: 451nm, Black: RGB.*

The performance for all MM elements evaluated together is given in Figure 4. When all MM elements are used simultaneously for classification the residual of the i.i.d. Gaussian model in Equation 10 is expected to be non-trivial for this 16-dimensional parameter set. Despite this simplified likelihood model the average AUC over all scatter angles are: 0.97 for red, 0.97 for green, 0.95 for blue, and for all color channels combined 0.97. The performance is saturated to AUC=1.0 at a majority of scatter angles. The decrease in AUC above 110° and below 50° in Figure 4 is attributed to an overly simplified likelihood model.

In Figure 5, the AUC of individual MM elements are shown. The m_{22} and m_{33} elements have the best performance across all angles measured. The AUC dependence on scatter angle is notable in elements m_{32} and m_{23} which increase drastically with scatter angle. Elements m_{32} and m_{23} relate to the transformation of diagonally polarized light into circularly polarized light. The AUC dependence on wavelength is notable in elements m_{20} and m_{30} where the larger wavelength from red performs poorly at lower scattering angles. Elements of the MM cannot be measured

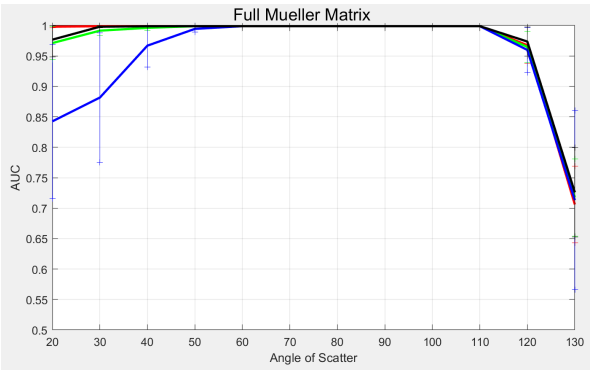

Figure 4. *Area under the curve (AUC) for all individual Mueller matrix elements. Average AUC is plotted with error bars indicating the 1st standard deviation. Red: 662nm, Green: 524nm, Blue: 451nm, Black: RGB.*

individually using a specific polarziation state generator and polarization state analyzer. A given MM element must be calculated from multiple measurements.

The AUC of diattenuation elements increases monotonically with scatter angle; see Figure 6. The average AUCs over all scatter angles are: 0.87 for red, 0.83 for green, 0.86 for blue, and 0.86 for combined RGB channels. There is not a statistically significance spectral dependence for the AUC of diattenuation.

The polarizance vector AUC has a very similar trends with scatter angle as the diattenuation vector; see Figure 7.The average AUCs over all scatter angles are: 0.88 for red, 0.84 for green, 0.87 for blue, and 0.87 for combined RGB channels. Neither diattenuation nor polarizance show a significant wavelength dependence in reported AUCs.

The remaining MM elements from the bottom-right corner of the full MM (defined as $\tilde{\mathbf{M}}$ in Equation eq:Mtilde) relate to both retardance and depolarization. In Figure 8 the average AUCs over all scatter angles are: 0.95 for red, 0.92 for green, 0.93 for blue, and 0.94 for combined RGB channels. At lower scatter angles, performance is nearly perfect. The decrease in performance for higher scatter angles has a minimum at 100° scattering angle.

The final parameter, depolarization, is computed from the depolarization index in Equation 7. Depolarization index is more effective than every preceding combination of the MM elements with AUC of 0.95 for red, 0.97 for green, 0.95 for blue, and 0.96 for the combined RGB channels. Only the Bayesian observer operating on all sixteen elements of the MM used simultaneously outperforms results from operating on the depolarization index. However, where AUC for all sixteen elements suddenly drops to the lowest AUC of 0.72 at the highest scatter angle, the depolarization index AUC is 1.00. The depolarization index AUC only drops to the lowest value of 0.85 at the two smallest scatter angles.

Conclusions

The Bayesian ideal observer demonstrates improved material classification when operating on polarization data compared to only irradiance data for images of white painted wood and white fabrics. Polarization data classification does not rely on the context of material within an image scene to make accurate classifications. Instead, polarimetric measurements quantify optical properties of the material. When used individually as classifica-

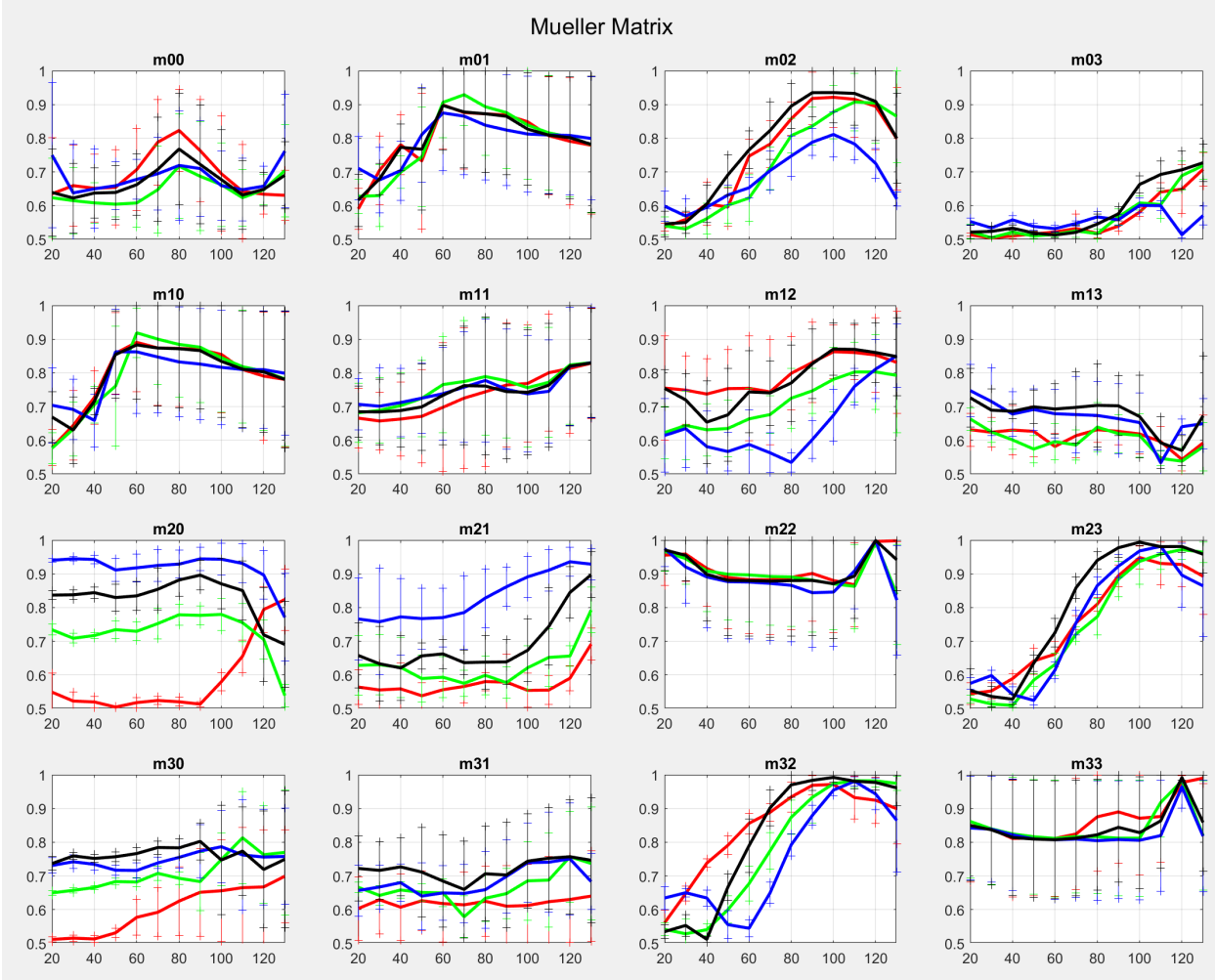

Figure 5. *Area under the curve (AUC) for each individual Mueller matrix element. Average AUC is plotted with error bars indicating the 1st standard deviation. Red: 662nm, Green: 524nm, Blue: 451nm, Black: RGB. Element m00 is equivalent to the traditional irradiance image benchmark.*

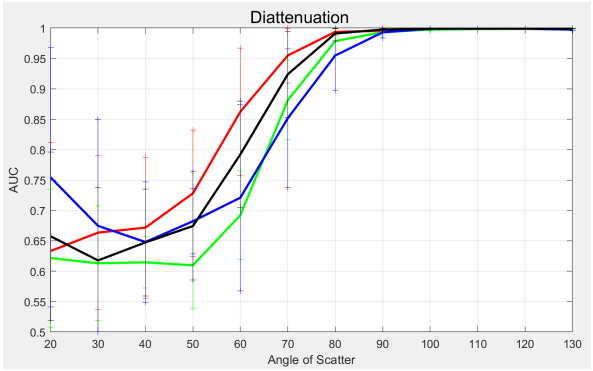

Figure 6. *Area under the curve (AUC) for irradiance and the diattenuation vector. Average AUC is plotted with error bars indicating the 1st standard deviation. Red: 662nm, Green: 524nm, Blue: 451nm, Black: RGB*

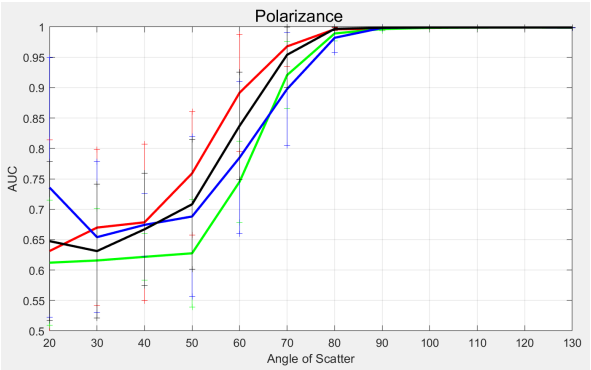

Figure 7. *Area under the curve (AUC) for irradiance and the polarizance vector. Average AUC is plotted with error bars indicating the 1st standard deviation. Red: 662nm, Green: 524nm, Blue: 451nm, Black: RGB*

tion parameters individual MM elements do not outperform traditional RGB imaging. This suggests that maximizing the material classification improvement from polarization imaging is possible without a full MM measurement. No single polarization parameter on its own functions as a perfect classifier across all scatter angles. In this work, objects are measured at specular scatter an-

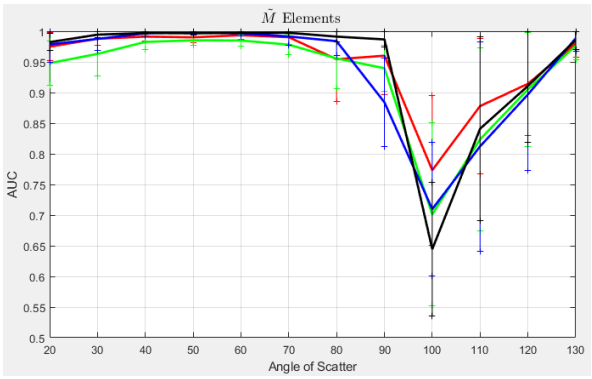

Figure 8. *Area under the curve (AUC) for $\tilde{\mathbf{M}}$ elements. Average AUC is plotted with error bars indicating the 1st standard deviation. Red: 662nm, Green: 524nm, Blue: 451nm, Black: RGB.*

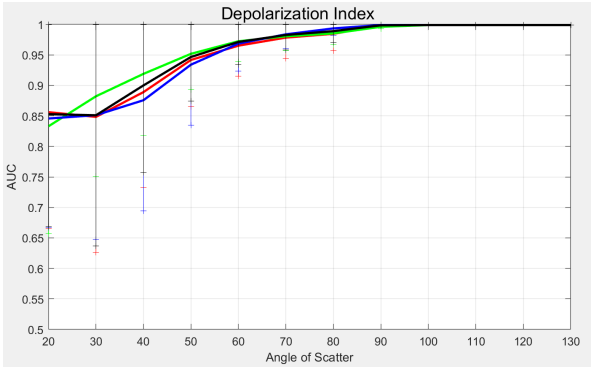

Figure 9. *Area under the curve (AUC) for depolarization index for each angle of incidence. Average AUC is plotted with error bars indicating the 1st standard deviation. Red: 662nm, Green: 524nm, Blue: 451nm, Black: RGB.*

gles ranging from $20^\circ - 130^\circ$.

In this sample set, depolarization index is the highest performing parameter out of all tested polarization parameters for scatter angles $\geq 70^\circ$ where AUC$\geq$0.98. At its worst performance, the Bayesian observer reports an AUC of 0.83 for the green wavelength at 20° scatter angle. For RGB retardance AUC$\geq$98 from 20° to 90° scatter angle. The lowest AUC is 0.64 at 100°, but raises sharply at the highest scatter angles.

The Bayesian ideal observer reports similar AUC values for the polarizance data and the diattenuation data. For both polarizance and diattenuation, the AUC reported is > 0.95 for scatter angles greater than 80°. The lowest AUC of 0.61 ± 0.1 for both parameters is reported for the green wavelength for scatter angles 20° to 50°. A consistent AUC $\geq$ 0.99 can be achieved using a combination of $\tilde{\mathbf{M}}$ for scatter angles $\leq 80^\circ$ and polarizance for scatter angles $\geq 80^\circ$. Therefore, achieving perfect performance across multiple scatter angles using polarization parameters would still require the full MM to be captured.

References

[1] Lawrence B. Wolff, Classification Of Material Surfaces Using The Polarization Of Specular Highlights, Proc. SPIE, pg. 1005. (1989).

[2] S. Tominaga and Tetsuya Yamamoto, Metal-dielectric object classification by polarization degree map, International Conference on Pattern Recognition, 19, pg. 1-4. (2008).

[3] Hua Chen and L. B. Wolff, Polarization phase-based method for material classification and object recognition in computer vision, Proc. CVPR, pg. 128.(1996).

[4] L.J. Denes, M. Gottlieb, B. Kaminsky and Daniel Huber, Spectro-Polarimetric Imaging for Object Recognition, Proc. AIPR, 3240. (1998).

[5] Subramaniam N., Saman G., Hancock E.R., Natural Material Segmentation and Classification Using Polarisation, Pattern Recognition and Image Analysis. (2011).

[6] F. Hu, Y. Cheng, L. Gui, L. Wu, X. Zhang, X. Peng, and J. Su, Polarization-based material classification technique using passive millimeter-wave polarimetric imagery, Appl. Optics, pg. 55. (2016).

[7] Takanori Nomura , Polarization imaging for 3D object recognition, SPIE. (2010).

[8] A. Mahendru and M. Sarkar, Bio-inspired object classification using polarization imaging, Sixth International Conference on Sensing Technology (ICST), pg. 207-212. (2012).

[9] Diane Hu, Liefeng Bo and Xiaofeng Ren., Toward Robust Material Recognition for Everyday Objects, Proc. British Machine Vision Conference, pg. 48.1-48.11. (2011).

[10] Sharan, L., Liu, C., Rosenholtz, R. et al.,Recognizing Materials Using Perceptually Inspired Features, Int J Comput Vis pg. 348. (2013).

[11] G. Schwartz and K. Nishino, Recognizing Material Properties from Images, IEEE Transactions on Pattern Analysis and Machine Intelligence. (2019).

[12] Bian, P., Li, W., Jin, Y. et al., Ensemble feature learning for material recognition with convolutional neural networks, Proc. J Image Video, pg. 64. (2018).

[13] J.M. López-Téllez, R.A. Chipman, L.W. Li, S.C. McEldowney, and M.H. Smith. Broadband extended source imaging Mueller-matrix polarimeter, Optics Letters, Vol. 44, Issue 7, pg. 1544-1547 (2019)

[14] S. Lu and R. Chipman. Interpretation of Mueller matrices based on polar decomposition, JOSA A, 13, 5, 1106. (1996).

[15] Meredith Kupinski, J. Bankhead, A. Stohn, and R. Chipman. Binary classification of Mueller matrix images from an optimization of Poincaré coordinates, JOSA A, 36, 6, 983. (2017).

[16] Russell Chipman, Wai Sze Tiffany Lam, and Garam Young. Polarized Light and Optical Systems. Boca Raton, FL. pg. 225-230 (2019).

[17] José Jorge Gil and Eusebio Bernabeu. Depolarization and Polarization Indices of an Optical System, Optica Acta: International Journal of Optics, 33, 2, pg. 185-189. (1986).

[18] H. H. Barrett, J. Yao, J. P. Rolland, K. J. Myers. Model observers for assessment of image quality, Proc. Natl. Acad. Sci. USA, 90, 21, pg. 9758-9765. (1993).

[19] Russell Chipman. Depolarization index and the average degree of polarization, Applied Optics, 44, 13, pg.2490-2495. (2005).

Author Biography

Lisa Li received the B.S.in Optical Sciences and Engineering from the University of Arizona in 2015 and the M.Sc. in computer science from Newcastle University in 2016. She is currently pursuing a Ph.D. in Optical Sciences at the University of Arizona. Her work focuses on the polarization properties of materials and material recognition.

Meredith Kupinski received the M.S. and Ph.D. degrees in Optical Science from the University of Arizona in 2003 and 2008, respectively. She is currently a Research Professor with the College of Optical Sciences, at the University of Arizona. Her research interests include task-relevant metrics for imaging system design, estimation/detection theory, and stochastic systems analysis and information quantitation.

Madellyn Brown is currently pursuing her B.S. in Optical Sciences and Engineering from the University of Arizona. She is an Undegraduate Research Assistant for the Polarization Lab where her work focuses on data acquisition and image analysis.

Russell A. Chipman received the B.S. in physics from the Massachusetts Institute of Technology and the M.S. and Ph.D. in Optical Science from the University of Arizona. He is currently a Professor of Optical Sciences with the University of Arizona and a Visiting Professor with the Center for Optics Research and Education at Utsunomiya University in Utsunomiya, Japan. He has coauthored the textbook Polarized Light and Optical Systems. Dr. Chipman is a fellow of The Optical Society (OSA) and The International Society for Optics and Photonics (SPIE). He received the SPIE 2007 G. G. Stokes Award for research in Polarimetry and the OSA Joseph Fraunhofer Award/Robert Burley Award for Optical Engineering in 2015.

JOIN US AT THE NEXT EI!

IS&T International Symposium on

Electronic Imaging

SCIENCE AND TECHNOLOGY

Imaging across applications . . . Where industry and academia meet!

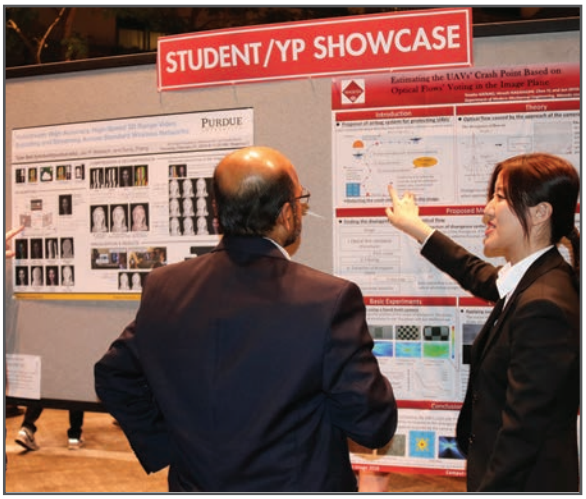

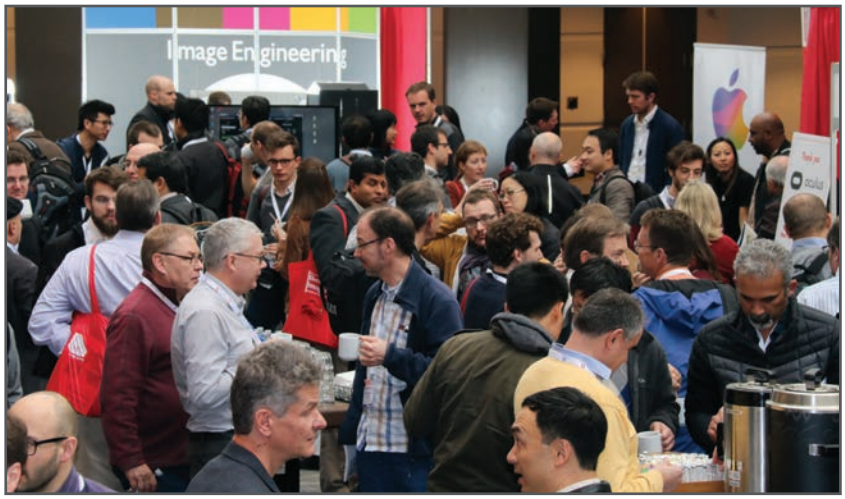

• SHORT COURSES • EXHIBITS • DEMONSTRATION SESSION • PLENARY TALKS •
• INTERACTIVE PAPER SESSION • SPECIAL EVENTS • TECHNICAL SESSIONS •

www.electronicimaging.org

IS&T
imaging.org